Photoemission and STM study of an In nanocluster array on the Si(111)-7×7 surface

J. H. Byun,[1] J. R. Ahn,[1,2] W. H. Choi,[1] P. G. Kang,[1] and H. W. Yeom[1,*]

[1]*Institute of Physics and Applied Physics and Center for Atomic Wires and Layers, Yonsei University, Seoul 120-746, Republic of Korea*

[2]*BK21 Physics Research Division and Sungkyunkwan University Advanced Institute of Nano Technology (SAINT), Sungkyunkwan University, Suwon 440-746, Republic of Korea*

(Received 12 May 2008; revised manuscript received 22 October 2008; published 13 November 2008)

The formation of nanoclusters for submonolayer indium on the Si(111)-7×7 surface was investigated by scanning tunneling microscopy (STM) and high-resolution photoelectron spectroscopy. The In 4*d* spectra indicate distinct bonding configurations for the well-known nanoclusters formed at 420–550 K and for the initial adsorbates at lower temperature. The STM imaging reveals a different type of clusters, with uniform shape and size, formed by the initial adsorbates. The spectral evolution of Si 2*p* indicates the importance of Si restatom sites for the formation of both initial clusters and nanoclusters in contrast to Si adatoms. The surface becomes semiconducting after the formation of the nanocluster array. For the well-developed nanoclusters, we found a surface state in valence bands at a binding energy of 0.6 eV. The origin of this surface state is discussed in comparison with a recent theoretical calculation.

DOI: 10.1103/PhysRevB.78.205314 PACS number(s): 73.20.At, 79.60.Dp, 68.43.Hn, 79.60.Jv

I. INTRODUCTION

In recent decades, supported nanoclusters on surfaces have been investigated extensively not only because of scientific interests but also because of potential applications for atomic-scale devices and catalysts. For example, nanosize Au clusters exhibit the extraordinary chemical reactivity for a useful catalysis.[1,2] It was suggested that the quantum-dot array can be used for single-electronic quantum-computing devices.[3] For most of these applications including also the ultrahigh-density magnetic recording media, the uniform size distribution and the highly ordered positioning are important.[4]

So far, various techniques have been applied to fabricate a well-ordered nanocluster array, and the self assembly on surfaces has been one of the most successful methods. In particular, the Si(111)-7×7 surface superstructure has been successfully employed to get highly ordered self-assembled arrays of identically sized nanoclusters for group-III metals (Al, Ga, In, and Tl), and Pb.[5–14] Other metals such as Ag, Au, Cu, Na, Co, Mn, and Fe,[15–23] and semiconductor elements such as Si and Ge (Refs. 24–26) also form nanocluster arrays on this surface but with lower degree of orders in sizes and positions.

The atomic structures of group-III nanoclusters have been extensively studied by scanning tunneling microscopy (STM) and first-principles theoretical calculations. According to the prevailing structural model, six metal atoms together with three *displaced* Si adatoms form a characteristic nine-atom planar cluster within a half-unit cell of 7×7 (see Fig. 1 for the schematics).[8] This structure reduces the number of surface dangling bonds significantly to provide a sufficient energetic motivation for the nanocluster formation. However, irrespective of the crucial importance in various applications, the chemical and electronic properties of these nanocluster arrays have not been made clear with only very few experimental studies.[7,20]

In this paper, we investigated the evolution in structures, bonding configurations, and electronic properties of the In nanocluster on the Si(111)-7×7 surface as functions of temperature and coverage by STM and core-level and valence-band photoelectron spectroscopy. The clearly different bonding configurations for initial adsorbates and nanoclusters are disclosed. The initial adsorbates form a distinct type of clusters with a rather uniform structure, which could be the precursory state of the nanoclusters. The valence-band spectra reveal the semiconducting property of the nanoclusters, which is consistent with a recent calculation.[27]

II. EXPERIMENTAL DETAILS

STM measurements were carried out with a commercial variable-temperature STM (Omicron, Germany) at room temperature (RT). Photoelectron spectroscopy measurements were performed at the undulator beamline 8A1 in Pohang

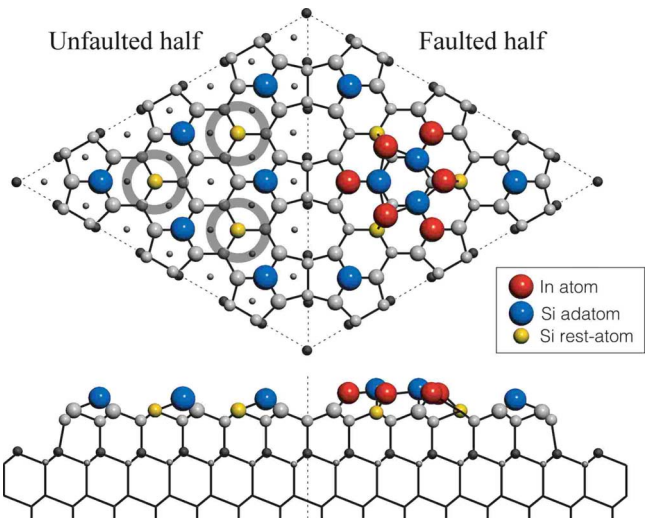

FIG. 1. (Color online) Schematics of the atomic structure model for the In nanocluster on the Si(111)-7×7 unit cell (Ref. 8). The gray rings around the restatoms indicate the highly stable adsorption sites (so-called basin sites) (Ref. 31).

Accelerator Laboratory (Pohang, Korea) using high-performance hemispherical electron analyzer (SES-2002, Gammadata, Sweden). Most of the spectra are angle integrated, otherwise specified as angle resolved, over the full acceptance angle of the analyzer, $\pm 8°$. In the case of angle-resolved measurement for valence bands, the angular resolution was about 0.2°. The clean Si(111) surface was prepared by postannealing at 850 °C after flash annealing at 1230 °C by direct current flow. The 7×7 ordering of the Si surface was checked by low-energy-electron diffraction (LEED) and the well-established Si $2p$ photoelectron spectrum.[28] Indium was deposited from a graphite effusion cell. The sample temperature was controlled by liquid-nitrogen cooling and an indirect feedback heater below 500 K or by direct resistive heating above. The temperature was measured by both an optical pyrometer with the emissivity setting of 0.63 and a thermocouple attached to the sample holder. The possible temperature difference between the sample holder (the thermocouple reading) and the sample surface was calibrated by the optical pyrometer above 800 K, which was extrapolated to 500 K. The difference at a lower temperature was marginal. The deposition rate of the evaporator was confirmed to be constant by measuring the In $4d$ photoelectron intensities. Thus, the relative In coverage could be controlled by the deposition time. The absolute In coverage [below 1 monolayer (ML)] was calibrated by the In $4d$ intensities for the well-ordered Si(111)4×1-In and Si(111)$\sqrt{3}\times\sqrt{3}$-In surfaces with the nominal coverages of 1.0 and 0.33 ML, respectively.[29]

III. RESULTS AND DISCUSSION

The template for the nanocluster formation, that is, the unit cell of the Si(111)-7×7 surface is separated with faulted-half-unit cells (FHUCs) and unfaulted-half-unit cells (UHUCs) by the stacking fault between the second and third layers. Each half-unit cell has six adatoms and three restatoms with single unpaired electrons or dangling bonds.[30] The previous theoretical studies reported that the highly coordinated sites around restatoms (shown by circles in Fig. 1) are the most stable adsorption sites for group-III metal adsorbates.[31] When the temperature goes up to 370–490 K, metal adsorbates partially reconstruct the surface structure to form nanoclusters; as mentioned above, six metal atoms and three center Si adatoms form a triangular nanocluster within a half-unit cell while keeping the 7×7 surface periodicity (see Fig. 1).[8] The corresponding STM images are shown in Figs. 2(a) and 2(b). The Si restatoms are directly bonded to metal atoms and the center adatoms within the nanocluster are displaced. The triangular protrusions with strong contrast in the STM images [inset of Fig. 1(a)] correspond to the six In adatoms. It was also reported that FHUCs were more favored in the nanocluster formation than UHUCs. This preference is so remarkable that more than 90% of nanoclusters could be formed at FHUCs at 0.12 ML.[11] This behavior is very clear in our own STM images with 0.10 ML [Figs. 2(a) and 2(b)]. As the coverage of metal adsorbates increases over 0.12 ML, the UHUCs start to be occupied and the surface is fully covered by nanoclusters at 0.24 ML. When both half-unit cells are occupied, this reconstruction reduces the number of dangling bonds in a 7×7 unit cell from 19 to 7 (six corner adatoms and one corner hole atom do not participate in the nanocluster formation).

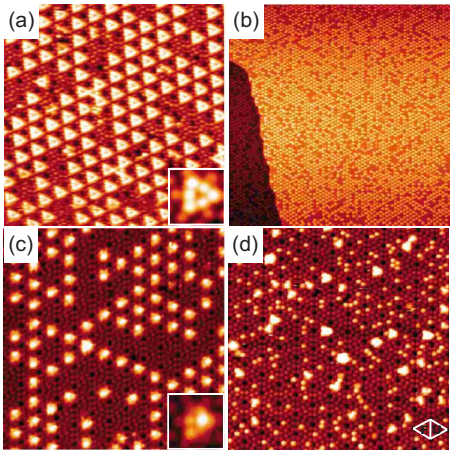

FIG. 2. (Color online) STM image (30×30 nm^2) of (a) the Si(111)-7×7 surface with 0.10 ML of In deposited at RT and annealed at 500 K, and (b) the same surface in a wider view (180×180 nm^2). Similar image for (c) 0.08 ML of In deposited at RT and (d) after annealing at 700 K. Sample bias voltages are +1.0 V for (a) and (b), and +1.8 V for (c) and (d). The tunneling current of all images is 50 pA.

Figure 3 is the evolution of In $4d$ photoemission spectra as the In coverage increases from 0.08 to 0.53 ML. Indium was deposited at 160 K and postannealings were performed at 500 K, which was the optimized temperature for the nanocluster formation in our own measurement. The 0.25 ML spectrum in circles at the middle of Fig. 3 is from the sample for which In is deposited at 500 K. It shows basically no difference from the postannealed case. The In $4d$ core level shows a well-resolved spin-orbit doublet below 0.44 ML with the energy splitting between $4d_{3/2}$ and $4d_{5/2}$ of 0.85 eV. At the coverage range up to 0.25 ML, the spectral line shape is rather invariant, which is asymmetric with a barely noticeable shoulder feature (denoted as C) at the lower binding-energy side. Above 0.25 ML, the main peak gradually shifts to a lower binding energy. The energy position of the main peak and the developed shoulder at 0.53 ML are consistent with those of the characteristic In $4d$ components (so-called α and β) for the Si(111)4×1-In surface formed at this temperature at nominally 1.0 ML.[29,32,33] From this behavior, we deduce that the N component is due to the nanoclusters formed below ~0.3 ML, and the surface at a higher coverage is a mixture of the nanoclusters and the 4×1-In domains. The origin of the minor component C is discussed below.

In order to confirm that the N component is due to In nanoclusters, we tracked the temperature dependence of In $4d$ spectra. Indium atoms of 0.24 ML were initially deposited on Si(111)-7×7 at 160 K and postannealed at temperatures of 360–790 K. This coverage corresponds to the full saturation of all available 7×7 half-unit cells. When the temperature was increased over 790 K, the desorption of In atoms started, as observed by the drastic intensity decrease in In $4d$ spectra (data not shown here). The evolution of the spectral

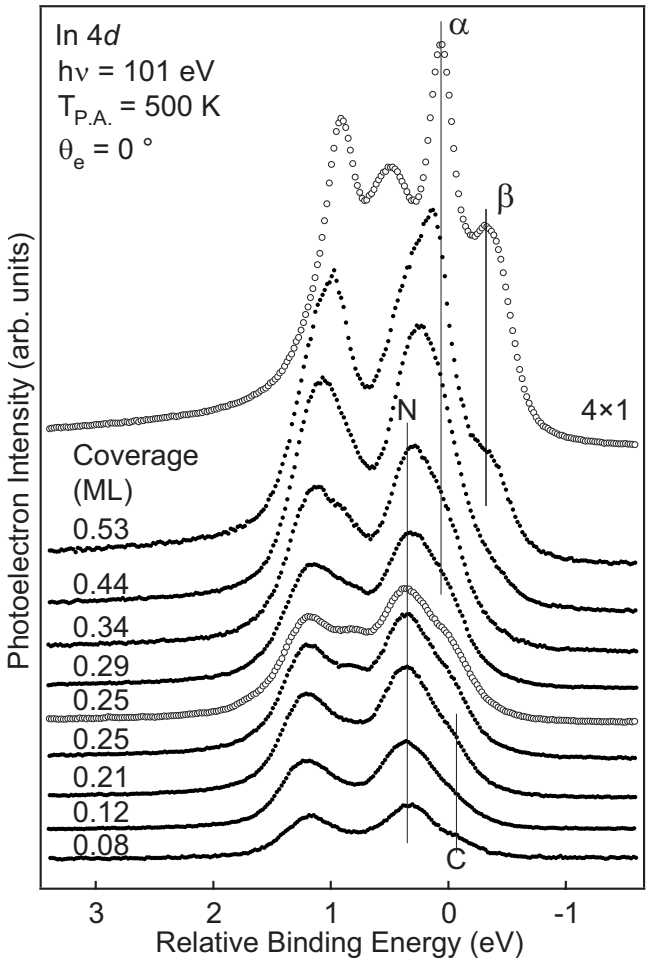

FIG. 3. In 4*d* photoelectron spectra for various In coverages on Si(111)-7×7 after annealing at 500 K. The spectra are taken with a photon energy ($h\nu$) of 101 eV at the normal emission. The topmost spectrum is from the Si(111)4×1-In surface, which is scaled by 0.5. The 0.25 ML spectrum in circles at the middle is from the sample for which In is deposited at 500 K.

line shape shown in Fig. 4 apparently defines three temperature ranges; the spectra are dominated by the component *A* below ~400 K, and by the *N* component mentioned above up to ~600 K, which is then replaced by the *C*′ component at higher temperatures.

The representative spectra for these temperature ranges were analyzed further through least-squares curve fittings as shown in Fig. 4(b). The spectra were fitted with integral backgrounds and minimum numbers of spin-orbit doublets ($4d_{3/2}$ and $4d_{5/2}$) given in Voigt functions. The existence of these components is qualitatively indicated by the apparent line shapes, as discussed above, and is quantitatively supported by the good-of-fit values of the fittings, which become order-of-magnitude worse when fewer components are used. The Lorentzian width of 0.17 eV and the spin-orbit splitting of 0.85 eV were used.[34] The detailed fitting parameters are given in Table I. In the 160 K spectrum, one dominant component (*A*) and two minor components (*A*′ and *A*″) were resolved. These minor components indicate that the adsorption site at low-temperature range is not unique. After the postannealing at 500 K, the *N* component shown in Fig. 3

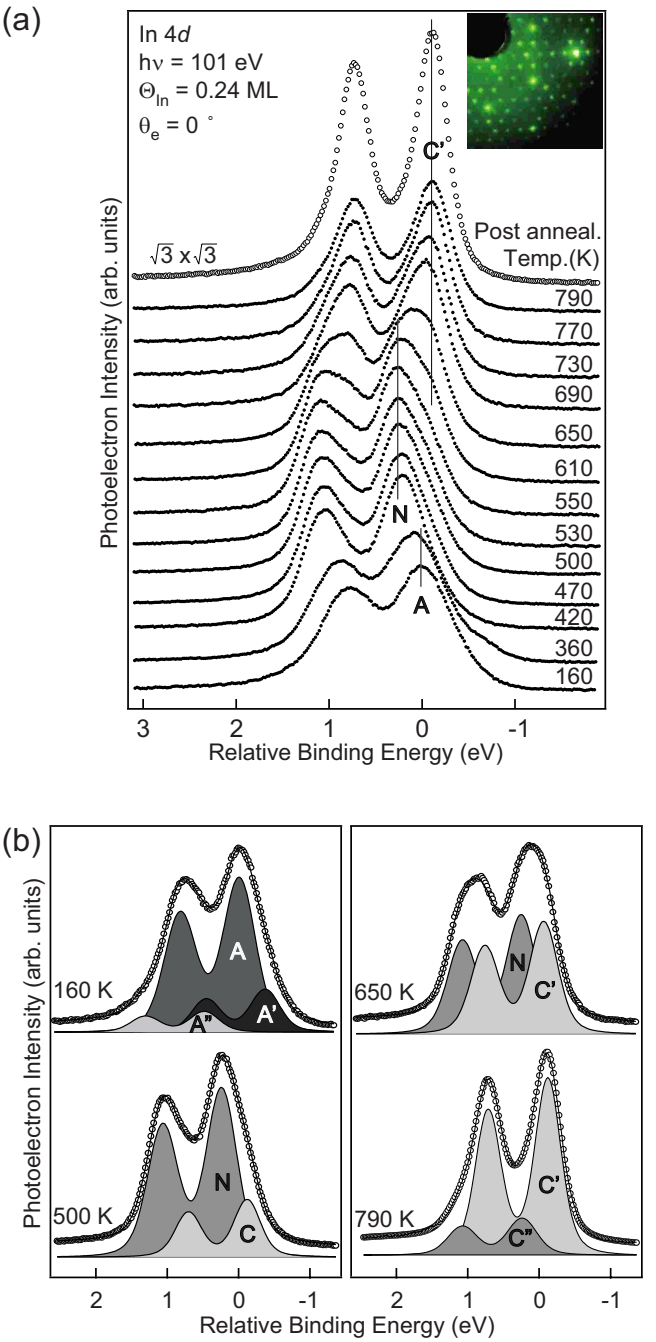

FIG. 4. (Color online) (a) In 4*d* photoelectron spectra for different postannealing temperatures after the In deposition of 0.24 ML on Si(111)-7×7 at 160 K. The spectra are taken with a photon energy ($h\nu$) of 101 eV at the normal emission. The topmost spectrum is from the Si(111)$\sqrt{3}\times\sqrt{3}$-In surface as a reference. The inset is the LEED pattern after the 790 K annealing, which shows the mixture of the 7×7 and $\sqrt{3}\times\sqrt{3}$-In phases. (b) Decompositions, by least-squares curve fittings, of In 4*d* spectra at 160, 500, 650, and 790 K from (a). The results of the fits (solid lines) are overlaid on the raw data (circles).

dominates at 0.3 eV higher binding energy than *A*. All the binding energies are refereed to that of the *A* component hereafter. The shoulder feature *C* mentioned above is resolved at −0.1 eV. At a higher temperature, the *C*′ compo-

TABLE I. Optimized fitting parameters of In 4*d* spectra shown in Fig. 4(b). The intensities are relative integrated intensities for each component in fractions of the total integrated intensity. The core-level shifts (CLSs) are referred to that of the largest component in 160 K spectrum (*A*). The GWs are given and the Lorentzian width was optimized commonly at 0.17 eV. The spin-orbit split of 0.85 eV has been acquired from the well-known spectra for the $\sqrt{3}\times\sqrt{3}$-In and 4×1-In phases. The branching ratio (BF) values are also given.

Spectrum	Compt.	CLS (eV)	BR (eV)	GW (eV)	Intensity
160 K	*A*	0	0.76	0.45	0.69
	A′	−0.37	0.79	0.43	0.21
	A″	0.51	0.77	0.40	0.10
500 K	*N*	0.29	0.78	0.42	0.73
	C	−0.08	0.78	0.35	0.27
650 K	*N*	0.29	0.78	0.40	0.51
	C′	−0.04	0.80	0.38	0.49
790 K	*N*	0.28	0.78	0.40	0.16
	C′	−0.08	0.82	0.34	0.84

nent grows to dominate the spectra. However, since the binding energies of *A*, *C*, and *C′* are close and the intensity of *C* at the intermediate temperature range is not sufficiently large, it is not clear whether the *C* component is the residue of *A* of the lower temperature or the early stage of the *C′* component of the higher temperature. As a reference, we measured the In 4*d* spectrum for the well-ordered $\sqrt{3}\times\sqrt{3}$-In phase formed macroscopically at a similar In coverage (1/3 ML) at higher than 670 K [the spectrum at the top of Fig. 4(a)].[34] From this reference spectrum, the *C′* component can unambiguously be attributed to the $\sqrt{3}\times\sqrt{3}$-In domains. The formation of $\sqrt{3}\times\sqrt{3}$-In domains is corroborated from LEED showing a mixture of 7×7 and $\sqrt{3}\times\sqrt{3}$ patterns as shown in the inset of Fig. 4(a).

These results clearly indicate that (i) there exists a distinct initial adsorption stage below 400 K with a rather uniform bonding configuration represented by *A* (*A′*), (ii) the nanocluster formation occurs above 400 K as represented by *N*, and (iii) the $\sqrt{3}\times\sqrt{3}$-In domains form at a higher temperature than 600 K. The distinct difference in binding energy between the *A* and *N* components suggests that the bonding configurations of the initial adsorbates and the nanoclusters are significantly different.

The distinct initial adsorption configuration is identified by the STM experiment. Figure 2(c) shows the Si(111)-7×7 surface with 0.08 ML of In adsorbed at RT. The initially adsorbed In atoms are also confined within 7×7 half-unit cells and form clusters with almost identical sizes and shapes. As shown in the inset, the initial cluster has an asymmetric shape with one strong protrusion. Due to the triangular symmetry of a 7×7 half-unit cell, the strong protrusions have three different orientations. These initial clusters are also preferentially formed in FHUCs. By annealing at 500 K, most of these clusters transform into nanoclusters as shown in Fig. 2(a). In this transformation, the number of clusters is roughly conserved indicating that each initial clusters has five or six In adatoms. The STM image after annealing at a higher temperature of 650 K [Fig. 2(d) for 0.08 ML] shows a mixture of a small number of irregular clusters and bright protrusions known as the In adsorbates substituting Si adatoms.[35] At high enough coverages, these substitutional In adatoms are thought to form the $\sqrt{3}\times\sqrt{3}$-In phase. This result confirms that there exist three distinct adsorption stages: the initial-cluster formation, the nanocluster formation, and the decomposition of the nanoclusters into the substitutional adatoms.

The formation of the initial clusters from a very low coverage is not consistent with the simple adsorption model proposed by the theoretical calculation mentioned above, where the single adsorbate sits on a near-restatom site.[31] While the atomic structure of the initial clusters is not clear at present, the different In 4*d* binding energy for the initial clusters indicates that they have a different bonding configuration from the nanoclusters. This suggests that the initial clusters may have a largely different structure from the nanoclusters as also indicated by the STM image. This seems consistent with the fact that the initial clusters are formed spontaneously at low temperature while the nanoclusters need thermal activation to be formed.

Figure 5 shows the change of Si 2*p* spectra as the In coverage increases at 160 K before (solid spectra) and after (dotted spectra) postannealings at 500 K. The spectrum at the bottom was obtained from the clean Si(111)-7×7 surface. The *B*, *S*1, *S*2, and *S*3 components, as decomposed by a standard curve-fitting analysis, were convincingly attributed to bulk Si atoms, back-bonded atoms to adatoms, restatoms, and adatoms, respectively.[28] The existence of the fifth component *S*4 was also established well but its origin is not clear yet.[28] Since the In-adsorbed surfaces at most of the coverages are not homogeneous at all with the coexistence of In clusters and bare 7×7 units, any quantitative core-level fitting analysis is significantly limited. We, thus, only qualitatively discuss the apparent spectral shape changes. At 160 K, the decrease in the *S*1 component is apparent, which makes the *S*3 component at the highest binding energy resolved better (indicated by dashed lines). One can also notice the decrease in the *S*2 restatom component. The major noticeable

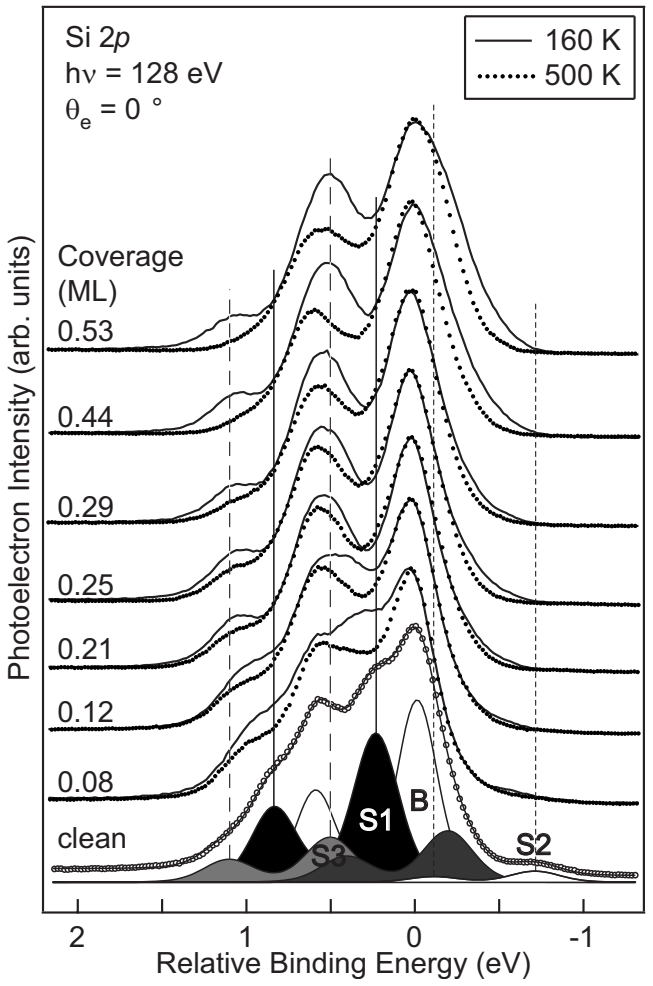

FIG. 5. Si $2p$ photoelectron spectra for increasing the In coverage from 0.08 to 0.53 ML on Si(111)-7×7 as deposited (solid lines) at 160 K and after annealings at 500 K (dotted lines). The spectra are taken with a photon energy ($h\nu$) of 128 eV at the normal emission. The spectrum at the bottom is from clean Si(111)-7×7 before In deposition. The result of the fits for the Si(111)-7×7 (solid lines) is overlaid on the raw data (circles).

change by annealings at low coverages is the decrease in $S1$, and that at high coverages, the decrease in $S3$. The disappearance of the restatom component $S2$ is consistent with the structure model of the nanocluster. Note also that the initial-cluster formation at low temperature similarly quenches $S2$. That is, the initial-cluster formation also actively involves the restatoms. In contrast, the adatom component $S3$ is largely intact except for high coverages. This contrasts with the behaviors of restatoms and indicates that the adatoms are not actively involved in In cluster formation. This is partly contradicting with the nanocluster structure model, where half of the adatoms are incorporated within the nanoclusters. The origin of this discrepancy is not clear at present. The disappearance of the adatoms at high coverage at high temperature is definitely due to the formation of the 4×1-In domains. The 4×1-In domains make the surface inhomogeneous, which may explain the broad structure appearing at the low binding-energy side at high coverages after annealing. On the other hand, the drastic change of the $S1$ component for the back-bonded atoms is not straightforwardly explained but may be attributed to the relaxation of the Si surface layer by the In cluster formation.

Finally, we discuss the electronic structure of the nanoclusters. Figure 6 shows the changes of valence-band photoelectron spectra with increase in the postannealing temperature up to 790 K at the coverage of 0.24 ML, which corresponds to the core-level spectrum series of Fig. 4(a). The reference spectrum for the bare Si(111)-7×7 surface is also given, which exhibits the well-known surface states S_1 and S_2 for the dangling bonds on Si adatoms and restatoms, respectively.[28,36,37] As in the case of In $4d$ spectra, the change of valence-band spectra consistently shows three distinct temperature ranges, that is, below 400 K for the initial adsorption, between 420 and 550 K for the nanocluster formation, and above 600 K for the formation of the $\sqrt{3}\times\sqrt{3}$ phase. For the case of the initial adsorption at 160 K, it is notable that the adatom surface state S_1 is hardly affected while the intensity of the restatom surface state S_2 is strongly suppressed. This indicates clearly that the initial-cluster formation involves restatom sites in agreement with the Si $2p$ result shown in Fig. 5.[31]

At the temperature range for the nanocluster formation, the S_2 state is almost completely quenched at this coverage of 0.24 ML. Instead, a rather small peak appears at the binding energy of 0.6 eV and is denoted as S_N. This surface state may be related to the nanocluster formation. However, it shows an intriguing behavior: it loses intensity between 610 and 650 K but regains it at 690 K and seems to develop into the S_2' state above 700 K. It is thus not conclusive whether the S_N state is directly related to In nanoclusters or not. The appearance of the S_2' state at high temperatures is accompanied by the growth of yet another surface state S_3, which can be assigned as the well-known intrinsic surface state of the $\sqrt{3}\times\sqrt{3}$ phase.[38] This spectral change can be understood if we consider the fact that the growth of the $\sqrt{3}\times\sqrt{3}$ domains concomitantly makes the bare 7×7 domains as indicated by the LEED pattern [Fig. 4(a)]. That is, the S_2' state at high temperatures is actually the same as S_2, the restatom surface state.

Other than S_N, the nanocluster phase has no distinctive spectral feature in the whole valence-band energy range. We also scanned different emission angles of photoelectrons but fail to find any noticeable feature. The inset of Fig. 6(a) shows the spectral intensity near Fermi level (E_F) in more detail. On the clean surface, the spectral intensity at E_F is dominated by the adatom surface state S_1. This is due to the partial electron transfer from the adatom dangling bonds to the restatom dangling bonds.[39] This state is only marginally affected by the initial adsorption at low temperature, as mentioned above. As nanoclusters form at 400–600 K, the S_1 intensity decreases and its peak position shifts to a higher binding energy to saturate at about 0.2–0.3 eV. Note that S_1 represents two or three nearly degenerated adatom states with only small energy differences.[27] The remaining intensity is roughly half. This is consistent with the structure model, where half of the adatoms, i.e., the corner adatoms, are not involved in the cluster formation. For the adatom-saturated surface at 500–600 K, there is no spectral intensity at E_F, indicating that the surface becomes semiconducting and the

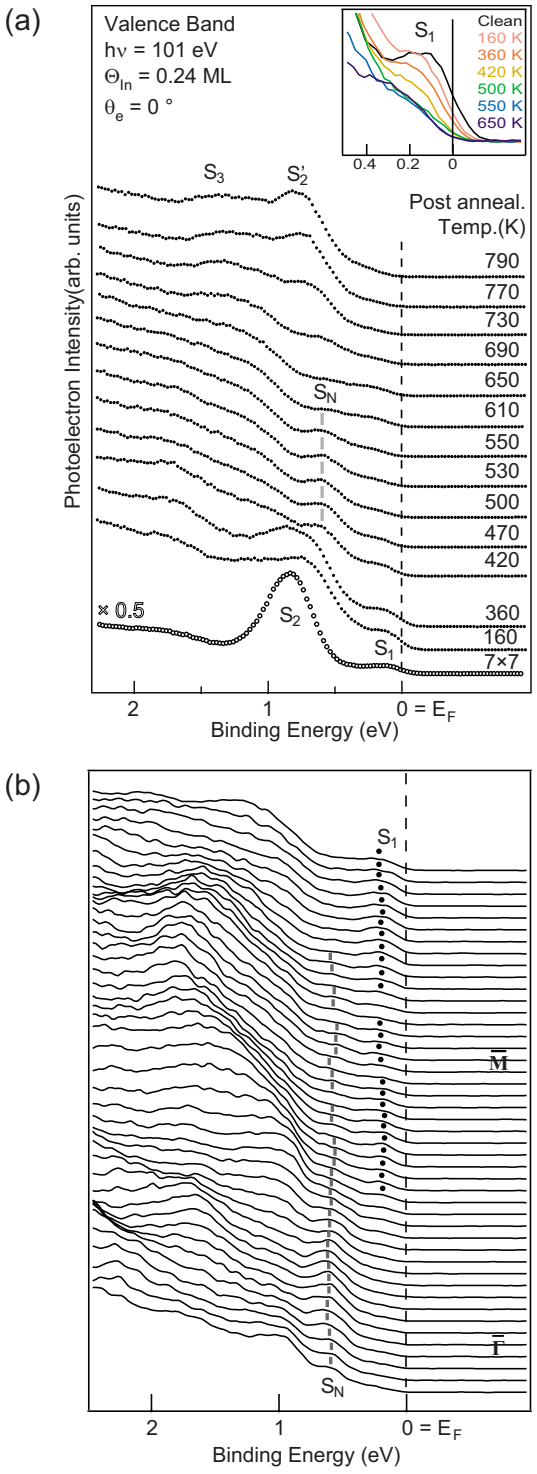

FIG. 6. (Color online) (a) Valence-band photoelectron spectra for increasing the postannealing temperature up to 790 K after an In deposition of 0.24 ML on Si(111)-7×7 at 160 K (the same series as the spectra of Fig. 4). The spectra are taken with a photon energy ($h\nu$) of 101 eV at the normal emission. The spectrum at the bottom is from clean Si(111)-7×7 before In deposition. The inset in (a) shows the evolution of the S_1 adatom state near the Fermi level in more detail. (b) Angle-resolved photoelectron spectra of the Si(111) surface with 0.24 ML of In after an annealing at 500 K. The spectra are taken with a photon energy ($h\nu$) of 101 eV along $[11\bar{2}]$ direction ($\bar{\Gamma}$-$\bar{M}$ in the 1×1 surface Brillouin zone).

nanoclusters do not have their own metallic electron state. Figure 6(b) is the angle-resolved photoelectron spectra of the surface after 500 K annealing with 0.24 ML of In along the $\bar{\Gamma}$-$\bar{M}$ direction in the 1×1 Brillouin zone. It clearly shows almost no dispersion for the S_N state, indicating that this state is a well-localized fully occupied state. There is no other feature dispersing toward E_F while one can find the remaining S_1 state near E_F without a noticeable dispersion. Therefore, we can conclude that the nanoclusters are semiconducting.

The above result is corroborated by valence-band spectra taken at different coverages at the optimum temperature of 500 K for the nanocluster formation. Figure 7 shows the changes of the surface states at various coverages. S_1 and S_2 states decrease as the In coverage increases; S_2 is almost fully quenched at about 0.2 ML but a half of S_1's intensity survives at the nanocluster saturation coverage of 0.25 ML. The increase in the In coverage beyond 0.24 ML reduces the intensity of S_1 further, suggesting that the overdosed In adsorbates attack the unreacted corner adatoms. The S_N surface state appears only up to 0.25 ML and abruptly disappears at a higher coverage. At a higher coverage than 0.25 ML, no clear surface-state feature is observed, suggesting that the overdosed surface is disordered. Note also that all of the above spectral changes, especially the energy shifts, are not due to the band bending shift as evidenced by the consistent binding energy of the bulk related spectral features (see the vertical guide line in Fig. 7).

With the results discussed so far, it is possible that the surface state S_N is related to In nanoclusters. However, since the binding energy of S_N is very close to that of the restatom surface state S_2 and it reappears above 600 K when the S_2 state grows due to the recovery of the 7×7 domains, one should be more careful in assigning the origin of S_N. So far, there is only one theoretical calculation for the electronic structure of group-III nanoclusters.[27] This work calculated the full band dispersions for 0.24-ML Al clusters and 0.12-ML In clusters. We adapted these results and simulated the measured (momentum-integrated) density of states by introducing the Gaussian broadening for the experimental energy resolution and the thermal effect. The Gaussian full width at half maximum (GW) of each component was set to be 200 meV. The energy scale of the theory was expanded by 1.3 times and shifted rigidly by 0.15 eV to the high binding side to match the binding energies of the experimental features (especially those of S_1 and S_2). This artificial adjustment may compensate the well-known underestimation of the gap size in local-density approximations and the experimental uncertainty in the E_F position due to the interfacial process such as band bending. The simulated results for nanoclustered and bare surfaces are given at the bottom of Fig. 7. The hatched and filled components are due to adatoms and restatoms (or corner holes), respectively. The other higher binding-energy states are due to Si-Si σ bonds and the In p-electron contributions are located out of the energy window of Fig. 7 due to strong bonding with Si atoms. The quenching of the restatom surface state is well reproduced in the theory. The state due to corner holes can be seen after the nanocluster formation at ~0.8 eV. This state may explain S_N

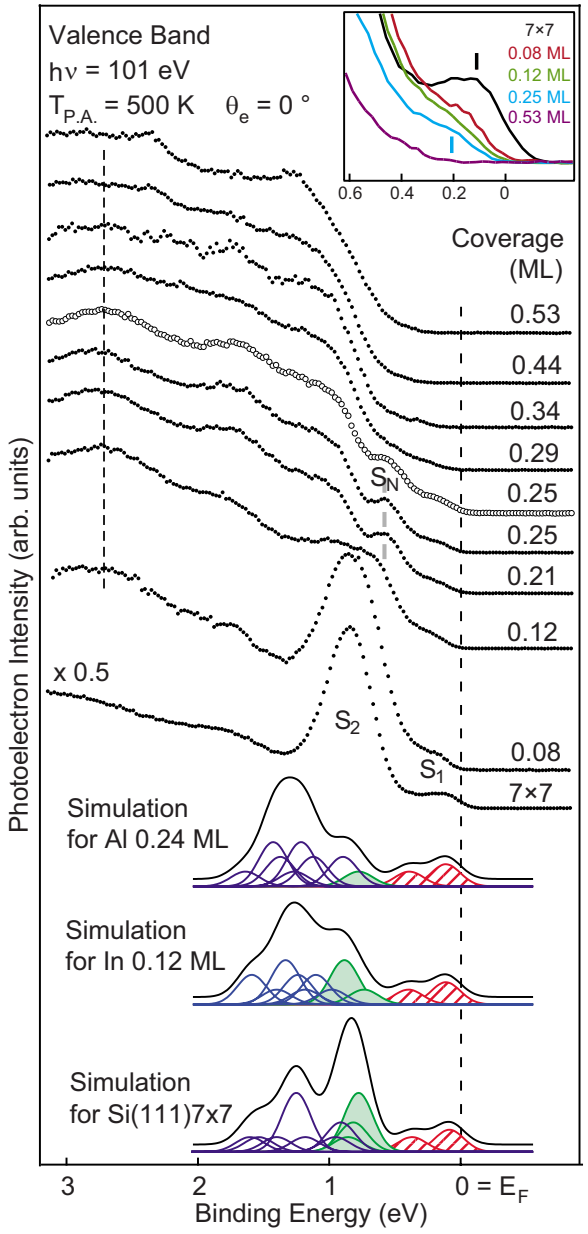

FIG. 7. (Color online) Valence-band photoelectron spectra for increasing the In coverage from 0.08 to 0.53 ML on Si(111)-7×7 after annealing at 500 K (the same series as the spectra of Figs. 3 and 5). The spectra are taken with a photon energy ($h\nu$) of 101 eV at the normal emission. The 0.25 ML spectrum in circles at the middle is from the sample for which In is deposited at 500 K. This spectrum is consistent with the postannealed case. At the bottom are the simulated valence bands for clean Si(111)-7×7, 0.12 ML of In-nanoclustered, and 0.24 ML of Al-nanoclustered surfaces based on the previous theoretical calculation (Ref. 27). The inset shows the evolution of the S_1 state as a function of the In coverage.

observed in the experiment. Another possible origin of S_N is the Si corner adatom state; the corner adatom state on Si(111)-7×7 was reported at ~0.5 eV in the previous experiments.[36,40] However, the present calculation gives the remaining adatom surface states at 0.1–0.4 eV, deviating from S_N. In order to understand the origin of the S_N state, a further investigation on local electronic structures is needed through a scanning tunneling spectroscopy (STS) experiment.

While the theory is consistent with the experiment in the semiconducting nature of the nanocluster itself, it has a noticeable discrepancy with the experiment for the adatom surface state S_1. In the theory, it was predicted that the occupied Si adatom dangling-bond states exhibit almost no change even after the nanoclusters are formed in clear contrast with the experiment (see the hatched components in the simulations of Fig. 7).[27] This may make the nanoclustered surface still metallic not due to the electronic states of the nanoclusters themselves but due to the remaining Si adatom dangling bonds. This is due to the fact that adatoms on the bare 7×7 surface donates dangling-bond electrons to restatoms but they are back donated after the nanoclusters saturate the restatom dangling bonds.[27,39] That is, although the number of adatoms with dangling bonds decreases by the nanocluster formation, the number of adatom dangling-bond electrons is almost intact in theory. However, the present experiment does not support this electron back donation and shows that half of adatom states are quenched to make the surface semiconducting by the formation of nanoclusters.

IV. SUMMARY

We investigated the adsorption and the cluster formation of In on the Si(111)-7×7 surface by STM, and core-level and valence-band photoelectron spectroscopy. The annealing temperature range of 160–800 K and the In coverage range of 0.08–0.6 ML were scanned since the formation of a well-ordered nanocluster array was reported at 400–500 K and 0.12–0.24 ML.

Through the evolution of In 4*d* spectra, distinct bonding configurations were resolved for nanoclusters and initial adsorbates at lower temperatures. STM reveals that the initial adsorbate forms uniform-sized clusters within the 7×7 half-unit cell whose structure is largely different from that of high-temperature nanoclusters. The Si 2*p* result shows the characteristic evolution of line shapes for the adatom, restatom, and back-bond atom components. It is indicated that the restatoms and the back-bond atoms are largely affected by both the initial-cluster and nanocluster formations in contrast to the largely intact adatoms. These behaviors indicate the importance of the restatom sites for the cluster formation at both low and high temperatures.

The valence-band spectra show that the nanoclustered surface is semiconducting with a band gap of 0.2–0.3 eV below the Fermi level. The electron back donation to the remaining adatom dangling bonds from the restatoms, predicted in the recent theory, is not observed.[27] A characteristic surface state is observed at 0.6 eV for the nanoclustered surface, which is thought to originate from the corner adatom dangling bonds or the corner hole dangling bonds.

ACKNOWLEDGMENTS

This work was supported by MOST through Center for Atomic Wires and Layers of the CRi program.

*Author to whom correspondence should be addressed; yeom@yonsei.ac.kr

[1] Masatake Haruta, Catal. Today **36**, 153 (1997).
[2] M. Valden, X. Lai, and D. W. Goodman, Science **281**, 1647 (1998).
[3] A. O. Orlov, I. Amlani, G. H. Bernstein, C. S. Lent, and G. L. Snider, Science **277**, 928 (1997).
[4] Shouheng Sun, C. B. Murray, Dieter Weller, Liesl Folks, and Andreas Moser, Science **287**, 1989 (2000).
[5] J.-F. Jia, J.-Z. Wang, X. Liu, Q.-K. Xue, Z.-Q. Li, Y. Kawazoe, and S. B. Zhang, Appl. Phys. Lett. **80**, 3186 (2002).
[6] V. G. Kotlyar, A. V. Zotov, A. A. Saranin, T. V. Kasyanova, M. A. Cherevik, I. V. Pisarenko, and V. G. Lifshits, Phys. Rev. B **66**, 165401 (2002).
[7] Run-Wei Li, Hongjun Liu, J. H. G. Owen, Y. Wakayama, K. Miki, and H. W. Yeom, Phys. Rev. B **76**, 075418 (2007).
[8] M. Y. Lai and Y. L. Wang, Phys. Rev. B **64**, 241404(R) (2001).
[9] Akihiro Ohtake, Phys. Rev. B **73**, 033301 (2006).
[10] J.-L. Li, J.-F. Jia, X.-J. Liang, X. Liu, J.-Z. Wang, Q.-K. Xue, Z.-Q. Li, J. S. Tse, Z. Zhang, and S. B. Zhang, Phys. Rev. Lett. **88**, 066101 (2002).
[11] J.-F. Jia, X. Liu, J.-Z. Wang, J.-L. Li, X. S. Wang, Q.-K. Xue, Z.-Q. Li, Z. Zhang, and S. B. Zhang, Phys. Rev. B **66**, 165412 (2002).
[12] L. Vitali, M. G. Ramsey, and F. P. Netzer, Phys. Rev. Lett. **83**, 316 (1999).
[13] Eric Ganz, Fulin Xiong, Ing-Shouh Hwang, and Jene Golovchenko, Phys. Rev. B **43**, 7316 (1991).
[14] S. C. Li, J. F. Jia, R. F. Dou, Q. K. Xue, I. G. Batyrev, and S. B. Zhang, Phys. Rev. Lett. **93**, 116103 (2004).
[15] St. Tosch and H. Neddermeyer, Phys. Rev. Lett. **61**, 349 (1988).
[16] Ivan Ošt'ádal, Pavel Kocán, Pavel Sobotík, and Jan Pudl, Phys. Rev. Lett. **95**, 146101 (2005).
[17] S. K. Ghose, P. A. Bennett, and I. K. Robinson, Phys. Rev. B **71**, 073407 (2005).
[18] Chun Zhang, Gang Chen, Krdong Wang, Hongwei Yang, Tao Su, C. T. Chan, M. M. T. Loy, and Xudong Xiao, Phys. Rev. Lett. **94**, 176104 (2005).
[19] K. Wu, Y. Fujikawa, T. Nagao, Y. Hasegawa, K. S. Nakayama, Q. K. Xue, E. G. Wang, T. Briere, V. Kumar, Y. Kawazoe, S. B. Zhang, and T. Sakurai, Phys. Rev. Lett. **91**, 126101 (2003).
[20] J. R. Ahn, G. J. Yoo, J. T. Seo, J. H. Byun, and H. W. Yeom, Phys. Rev. B **72**, 113309 (2005).
[21] M. A. K. Zilani, Y. Y. Sun, H. Xu, Y. P. Feng, X. S. Wang, and A. T. S. Wee, Phys. Rev. B **72**, 193402 (2005).
[22] De-yong Wang, Li-jun Chen, Wei He, Qing-feng Zhan, and Zhao-hua Cheng, J. Phys. D **39**, 347 (2006).
[23] M. A. K. Zilani, Y. Y. Sun, H. Xu, G. W. Peng, Y. P. Feng, X.-S. Wang, and A. T. S. Wee, Surf. Sci. **601**, 2486 (2007).
[24] H. M. Guo, Y. L. Wang, H. W. Liu, H. F. Ma, Z. H. Qin, and H. J. Gao, Surf. Sci. **561**, 227 (2004).
[25] Feng-Chuan Chuang, Bei Liu, Cai-Zhuang Wang, Tzu-Liang Chan, and Kai-Ming Ho, Surf. Sci. **598**, L339 (2005).
[26] H. Asaoka, V. Cherepanov, and B. Voigtländer, Surf. Sci. **588**, 19 (2005).
[27] Lixin Zhang, S. B. Zhang, Qi-Kun Xue, Jin-Feng Jia, and E. G. Wang, Phys. Rev. B **72**, 033315 (2005).
[28] C. J. Karlsson, E. Landemark, Y.-C. Chao, and R. I. G. Uhrberg, Phys. Rev. B **50**, 5767 (1994).
[29] J. Kraft, M. G. Ramsey, and F. P. Netzer, Phys. Rev. B **55**, 5384 (1997), and references therein.
[30] K. Takayanagi, Y. Tanishiro, M. Takahashi, and S. Takahashi, J. Vac. Sci. Technol. A **3**, 1502 (1985).
[31] K. Cho and E. Kaxiras, Europhys. Lett. **39**, 287 (1997).
[32] H. W. Yeom, K. Horikoshi, H. M. Zhang, K. Ono, and R. I. G. Uhrberg, Phys. Rev. B **65**, 241307(R) (2002).
[33] J. R. Ahn, J. H. Byun, J. K. Kim, and H. W. Yeom, Phys. Rev. B **75**, 033313 (2007).
[34] S. W. Cho, K. Nakamura, H. Koh, W. H. Choi, C. N. Whang, and H. W. Yeom, Phys. Rev. B **67**, 035414 (2003).
[35] H. Hibino and T. Ogino, Phys. Rev. B **55**, 7018 (1997).
[36] R. I. G. Uhrberg, T. Kaurila, and Y.-C. Chao, Phys. Rev. B **58**, R1730 (1998).
[37] R. Losio, K. N. Altmann, and F. J. Himpsel, Phys. Rev. B **61**, 10845 (2000).
[38] J. M. Nicholls, P. Maartensson, G. V. Hansson, and J. E. Northrup, Phys. Rev. B **32**, 1333 (1985).
[39] John E. Northrup, Phys. Rev. Lett. **57**, 154 (1986).
[40] J. Mysliveček, A. Stróżecka, J. Steffl, P. Sobotík, I. Oštádal, and B. Voigtländer, Phys. Rev. B **73**, 161302(R) (2006).